Microsc. Microanal., page 1 of 12
doi:10.1017/S1431927615015597

Microscopy AND Microanalysis

Time-Lapse Evaluation of Interactions Between Biodegradable Mg Particles and Cells

Florencia Alvarez,[1,†] Rosa M. Lozano Puerto,[2] Blanca Pérez-Maceda,[2] Claudia A. Grillo,[1] and Mónica Fernández Lorenzo de Mele[1,3,*]

[1]*Instituto de Investigaciones Fisicoquímicas Teóricas y Aplicadas (INIFTA), 1900 La Plata, Argentina*
[2]*Cell-Biomaterial Recognition Group, Cellular and Molecular Biology Department, Centro de Investigaciones Biológicas (CIB-CSIC), 28040 Madrid, Spain*
[3]*Facultad de Ingeniería, Universidad Nacional de La Plata, 1900 La Plata, Argentina*

Abstract: Mg-based implants have promising applications as biodegradable materials in medicine for orthopedic, dental, and cardiovascular therapies. During wear and degradation microdebris are released. Time-lapse multidimensional microscopy (MM) is proposed here as a suitable tool to follow, in fixed intervals over 24-h periods, the interaction between cells and particles. Results of MM show interactions of macrophages (J774) with the magnesium particles (MgPa) that led to modifications of cell size and morphology, a decrease in duplication rate, and cell damage. Corrosion products were progressively formed on the surface of the particles and turbulence was generated due to hydrogen development. Changes were more significant after treating MgPa with potassium fluoride. In order to complement MM observations, membrane damage as detected by a lactase dehydrogenase (LDH) assay and mitochondrial activity as detected by a WST-1 assay with macrophages and osteoblasts (MC3T3-E1) were compared. A more significant concentration-dependent effect was detected for macrophages exposed to MgPa than for osteoblasts. Accordingly, complementary data showed that viability and cell cycle seem to be more altered in macrophages. In addition, protein profiles and expression of proteins associated with the adhesion process changed in the presence of MgPa. These studies revealed that time-lapse MM is a helpful tool for monitoring changes of biodegradable materials and the biological surrounding in real time and *in situ*. This information is useful in studies related to biodegradable biomaterials.

Key words: biodegradation, magnesium, multidimensional microscopy, macrophage, osteoblast

Introduction

Orthopedic implants frequently generate debris that contributes to their aseptic loosening (Mirra et al., 1976; Jasty et al., 1986; Schmalzried et al., 1993; Maloney & Smith, 1995; Goodman et al., 1996). Periprosthetic granulomatous tissues retrieved from failed implants have been histologically analyzed and the presence of macrophages, lymphocytes, foreign body giant cells, and abundant particulate debris were detected (Harris et al., 1976; Dumbleton, 1981; Freeman et al., 1982; Johanson et al., 1987; Santavirta et al., 1991; Goldring et al., 1993; Schmalzried et al., 1993; Kang Jung et al., 1994; Horowitz & Purdon, 1995; Maloney & Smith, 1995). It is known that macrophages phagocytose orthopedic biomaterial particles and release pro-inflammatory mediators in response to particulate debris (Horowitz et al., 1988; Davis et al., 1993; Gelb et al., 1994; Glant & Jacobs, 1994; Horowitz & Gonzales, 1996; Nakashima et al., 1999; Trindade et al., 1999). Furthermore, macrophages interact with other cells present at the bone–implant interface to increase the release of pro-inflammatory mediators (Lind et al., 1998) and also may be involved in adhesion-dependent spontaneous apoptosis after interaction with biomaterials (Zachman et al., 2013). These effects have been recurrently analyzed in corrosion resistant debris (Caicedo et al., 2009; Posada et al., 2015). However, only a few reports are related to debris released by degradable metals (Bondarenko et al., 2011; Badar et al., 2013; Roth et al., 2014).

Mg-based materials are considered promising for orthopedic, dental, and cardiovascular applications (Goodman et al., 1996). The effect of Mg particles on UMR-106 cells was recently reported and toxic effects were particularly analyzed (Di Virgilio et al., 2011; Grillo et al., 2011). Cytotoxicity was found after exposure to magnesium particles (MgPa) at concentrations $\geq$1,000 μg/mL. On the other hand, Roth et al. (2014) reported that Mg debris is biocompatible and does not seem to restrict the immune function of macrophages at concentrations $\leq$500 μg/mL. Nevertheless, the analysis is complex because it is difficult to obtain the mass/volume relationships of the particles that are in contact with cells and degrade *in vivo*. In addition, fluids containing leached Mg seems to be an effective antiresorptive agent for the treatment of particle-induced osteolysis (Zhai et al., 2014). Thus, depending on the characteristics and concentration of Mg-containing products, beneficial or detrimental effects may be found.

Biocompatibility of Mg-containing metallic materials is mostly tested *in vitro* by replacing the supernatant culture medium of the cell culture by extracts. These extracts are

Received June 26, 2015; accepted November 20, 2015
*Corresponding author. mmele@inifta.unlp.edu.ar
† In memory of Florencia Alvarez (Flor) whose lovely life, plenty of fortitude, and spiritual values, we had the honor of sharing.

obtained after immersing the metal sample in the culture medium during selected periods. However, the use of magnesium particles (MgPa) is closer to the *in vivo* situation than the use of Mg salts or extracts because of factors such as local generation of bubbles, the space and time dependence of the concentration of corrosion products, as well as direct contact of cells with the particles and corrosion products that cannot be taken into account when extracts and Mg salts are used.

Considering that macrophages are one of the main biological factors that interact at the metallic debris/biological interface, it is interesting to investigate the effects of Mg particle interaction (with and without protective treatments with potassium fluoride) *in situ* with the macrophages.

There are several reports related to the interaction of cells with corrosion resistant debris (Hart et al., 2010; Gu et al., 2012; Ogunbileje et al., 2014; Zhai et al., 2014). However, to our best knowledge, the interaction of cells with degradable particles and with the corrosion products that are formed when the particles are in contact with the biological medium has not been analyzed in real time *in situ*.

Considering the biodegradable nature of Mg and its alloys that generate particles during their degradation, it can be inferred that the amount of debris will be enhanced in relation to traditional implants (Co-Cr, Ti, and Ti alloys) (Hart et al., 2010). Direct assays with cells in contact with the particles using time-lapse multidimensional microscopy (MM) allow us to mimic some aspects of the real situation and to obtain qualitative information about the changes in real time and *in situ* as a first step previous to *in vivo* assays.

It has been reported that debris dimension is an important factor when the effect of the particles is assayed. Debris size is frequently in the 5–70 μm range (Reddy et al., 2014). Mg particles, mesh 325, were used in this work and, accordingly, their diameters are different and shorter than 70 μm. Consequently, due to their dissimilar volumes their interaction with cells is probably different. In addition, it should be taken into account that, during the corrosion process, the mass of the particles decreases and some of them may be completely dissolved (Di Virgilio et al., 2011). To follow this dynamic process in real time we used MM. Thus, the effect of the degradation process, that is the formation of corrosion products, including bubbles development, could be detected and the different stages of these processes and their effect on cell growth were reported.

Several cellular and physicochemical processes involve fast transformations that could be followed by three-dimensional (3D) time-lapse microscopy (also called 4D microscopy or Multidimensional Microscopy (MM)). Faster, more robust and more sensitive equipment and algorithms for image and time-lapse processing have been published (Collins, 2007; Held et al., 2010; Baradez & Marshall, 2011; Huth et al., 2011). In time-lapse microscopy, images are recorded at fixed intervals over extended periods of time. 4D imaging should collect focal planes in time-lapse mode as rapidly as possible, without perturbing the sample by strong illumination or the use of staining. The original stack of 2D images is reconstructed into a 3D image that changes with time. This type of microscopy offers great functionality for biological, cytomorphological, and physicochemical examinations. Temperature stability, minimum exposure of specimens to light (protection from photobleaching), and highly sensitive recording techniques are frequently required to follow these processes. Thus, a climate chamber, cell chamber, CO_2 controller, and incubators must be included in the station when biological samples are analyzed. The resulting images and movies can provide direct insight into the behavior of cells including duplication, cell death, and migration among other processes (Baradez & Marshall, 2011; Huth et al., 2011).

MM is proposed here as a suitable tool to follow, at fixed intervals over 24-h periods, the interactions of particles, without or with fluoride coatings (MgPa and MgPa-F, respectively), with macrophages. Turbulence due to hydrogen development, gradual formation of corrosion products, and interactions with cells were evaluated *in situ*, in real time, by MM.

These MM observations were complemented by a comparative study of the response of a macrophage cell line (J774) and an osteoblast cell line (MC3T3-E1) in relation to membrane damage as detected by a lactate dehydrogenase (LDH) assay and mitochondrial activity as detected by a WST-1 assay after exposure to MgPa and MgPa-F. Additional information about changes in expression of proteins and cell cycle before and after exposure is also provided.

Materials and Methods

Cell Culture

Mouse osteoblasts (MC3T3-E1 cell line) and mouse macrophages (J774 cell line) were originally obtained from the cell bank of the Animal Cell Culture Facility of CIB (Centro de Investigaciones Biológicas, CIB, Madrid, Spain). Cells were grown in T-25 flasks with D-MEM culture medium (Gibco-BRL, Los Angeles, CA, USA) supplemented with 10% inactivated fetal calf serum, 100 IU/mL penicillin and 100 μg/mL streptomycin sulfate [complete culture medium, (CCM)] at 37°C in a 5% CO_2 humid atmosphere. Cells were counted using an improved Neubauer cell counting chamber (Carl Roth GmbH & Co., KG, Karlsruhe, Germany).

Mg Particles and Fluoride Treatment

MgPa (99.8%, 325 mesh, 58.9 ± 20.7 μm) were supplied by Alfa Aesar (Ward Hill, MA, USA) and were used to simulate Mg debris. Their chemical composition is reported in Table 1.

Some MgPa were treated with KF to test the effect of this corrosion protection treatment. Fluoride layers were generated on MgPa (MgPa-F) by immersion in 0.2 M KF solutions for 1 h at room temperature. The KF dose employed was

Table 1. Composition of the Mg particles.

Al	Si	Mn	Fe	Ca	Mg
0.030	0.031	0.019	0.015	0.110	Balance

selected taking into account the dose used for previous electrochemical studies that showed an inhibitory effect for KF treatment (Pereda et al., 2011). After the immersion period, MgPa-F were centrifuged and washed twice with sterile water, then suspended in CCM and subsequently added to the cell cultures. MgPa were used in the 250–2,000 μg/mL range. In *in situ* experiments in real time, the concentrations used were 1,000, 1,500, and 2,000 μg/mL.

Incorporation of F after KF treatment was detected by mass spectroscopy (Matrix Assisted Laser Desorption/ Ionization - Time-of-flight (MALDI-TOF)) analysis (data not shown) as evidence for the presence of fluoride layer on the MgPa-F.

All the chemicals used in the experiments were of analytical grade. Milli Pore-MilliQ water (Milli Pore, Darmstadt, Germany) was used to prepare the solutions.

MM *In Vivo*

Time-lapse microphotographs are very useful for following the formation of corrosion products as well as cell/MgPa interactions in real time. MM analysis was used to observe the interaction of J774 macrophages with Mg microparticles at 1,000, 1,500, and 2,000 μg/mL, and their corrosion products by the time-lapse sequence during 24 h. Cells cultured in eight multi-well plates with controlled parameters (37°C at 5% CO_2 and humid atmosphere) were observed with a Multidimensional microscope (Leica DMI6000B/AF-6000 LX, Leika Microsystems, Wetzlar, Hesse, Germany) connected to a CCD Hamamatsu C9100-02 (Hamamatsu Photonics, K.K., Hamamatsu, Japan) high resolution monochrome camera with a high speed acquisition (30 images/s) in real time.

LDH Leakage Assay

LDH is a stable cytoplasmic enzyme present in all cells and is involved in the conversion of lactate to pyruvate with parallel reduction of nicotinamide adenine dinucleotide. LDH is rapidly released into the cell-culture supernatant when the plasma membrane is damaged. To evaluate and quantify cell death and cell lysis, LDH activity was measured in the supernatants of cell cultures by an enzymatic assay using the Cytotoxicity Detection Kit (Roche Diagnostics, Barcelona, Spain) as described in Lozano et al. (2013). In this reaction the tetrazolium salt is reduced to a colored compound, formazan. The increase in supernatant LDH activity directly correlates to the amount of formazan formed over time.

For this analysis 2.5×10^3 cells/well were cultured in 24 multi-well plates and grown at 37°C in 5% CO_2 humid atmosphere, in CCM, for 24 h. Then the CCM was replaced by new media with different concentrations of MgPa or MgPa-F treatment. After 24 h exposure the enzymatic assays were performed on the supernatants according to the LDH kit (Roche Diagnosis) protocol. CCM was used as the background control. LDH activity was measured based on differential absorbance at 490–655 nm using a Bio-Rad iMark microplate reader (Bio-Rad Laboratories, Inc, Philadelphia, PA, USA). Cell culture controls (untreated cells, without particles) were also performed and a background control with CCM was used as an absorbance blank. A relative cytotoxicity percentage was calculated as $[(A–B)/A] \times 100$, where A and B correspond to the absorbance of control and treated cells, respectively. Each experiment was independently repeated three times. Data were analyzed using one-way analysis of variance (ANOVA) test and multiple comparisons were made using p values corrected by the Bonferroni method.

WST-1 Assay

This assay measures cleaved tetrazolium salt (WST-1) (4-[3-(4-Iodophenyl)-2- (4-nitrophenyl)-2H-5-tetrazolio]-1,3-benzene disulfonate (Roche Diagnostics, GmbH, Manheim, Germany) to formazan by dehydrogenase enzymes of mitochondria. The amount of formazan dye formed is directly correlated to the number of metabolically active cells in the culture.

For this analysis 2.5×10^3 cells/well were cultured in 24 multi-well plates and grown at 37°C in a 5% CO_2 humid atmosphere, in CCM, for 24 h. Then, CCM was replaced with other CCM with different concentrations of particles with (MgPa) and without (MgPa-F) KF treatment. After 24 h exposure, CCM was removed, cells were washed with phosphate buffered solution (PBS), and fresh medium containing WST-1 reagent (Cell Proliferation Reagent WST-1; Roche Diagnostics, Barcelona, Spain) was added and incubated for 3 h. Then the plate was shaken for 1 min and the absorbance of the samples was measured at 415–655 nm using a Bio-Rad iMark microplate reader. A background control with CCM was used as an absorbance blank. Negative controls (untreated cells) were run simultaneously in cultures without particles. A relative cytotoxicity percentage was calculated as $[(A - B)/A] \times 100$, where A and B are the absorbance of control and treated cells, respectively. Each experiment was independently repeated three times. Data were analyzed using one-way ANOVA test and multiple comparisons were made using p values corrected by the Bonferroni method.

Flow Cytometry (FC)

A comparative study of the effect of MgPa and MgPa-F and their degradation products on cell cycle and cellular viability of J774 and MC3T3-E1 cell lines analyzed by FC (XL Flow Cytometer; Beckman Coulter Corp., Brea, CA, USA) were included to complement MM information for illustrative purposes. Propidium iodide, which is a DNA intercalating fluorescent stain, was used. Briefly, cells (5×10^5 cells/well) were cultured in 12 multi-well plates at 37°C in a 5% CO_2 humid atmosphere, in CCM, for 24 h. Then, CCM was replaced by other CCM with 1,000 μg/mL of MgPa or MgPa-F and cultured for 24 h. After the exposure time, cell cultures were processed for FC as previously described (Lozano et al., 2013; Zachman et al., 2013). For comparative purposes we included the percentage of each cell in each cycle phase (subG_1, G_1, S, G_2/M) that was calculated using CXP software (Beckman Coulter Corp. Beckman Coulter, Inc., Brea, CA, USA).

Confocal Immunofluorescence Microscopy (CIM)

Data obtained by CIM were included to show the changes of vimentin and ICAM-1 after exposures to MgPa to complement the MM information. With this purpose MC3T3-E1 osteoblasts were seeded on sterile glass cover slips with 1 mL of CCM within a 12-well culture plate at a cell density of 2.5×10^3 cells/well and grown at 37°C in a 5% CO_2 humid atmosphere for 24 h. Then, CCM was replaced with other CCM with 1,000 μg/mL MgPa, and cells were maintained in culture for 24 h. For immunodetection assays, cells were fixed with 4% paraformaldehyde and with 2% powdered milk to block nonspecific binding of the primary antibody. Anti-vimentin (mouse monoclonal anti-mouse) (Cat. No. V5255; Sigma-Aldrich, St Louis, MO, USA) and anti-ICAM-1 (rabbit polyclonal anti-mouse) (Cat. No. sc-1511; Santa Cruz Biotechnology, Inc., Dallas, TX, USA) primary antibodies were used in 1:200 and 1:1,000 dilution in 2% powdered milk in PBS, respectively. Subsequently, incubations for 1 h at room temperature with each antibody were made. Alexa 488 anti-rabbit (Cat. No. A11008; Molecular Probes) at a 1:400 dilution in 2% powdered milk in PBS was used as the secondary antibody for ICAM-1 detection (green fluorescence) and Alexa 568 anti-mouse (Cat. No. A11004; Molecular Probes) at a 1:400 dilution was used as the secondary antibody in a solution of 2% powdered milk in PBS was used for vimentin detection (red fluorescence). Both were visualized by confocal microscopy (LEICA SP2 Confocal Scanning Microscopy, Wetzlar, Hesse, Germany). Cell nuclei were also stained with Hoechst 33258 (Sigma-Aldrich, St Louis, MO, USA) reagent by incubation for 10 min at room temperature with 1 mL of 2 μg/mL Hoechst 33258 (Doyle et al., 1995) in PBS and cell fluorescence was visualized by confocal microscopy.

Proteomic Profile Analysis

A comparative assay of the proteomic profiles of osteoblasts (MC3T3-E1) and macrophages (J774) before and after exposure of cells to 1,000 μg/mL of MgPa and MgPa-F was made. Briefly 5×10^5 cells/well were cultured in 12 multi-well plates and grown at 37°C in a 5% CO_2 humid atmosphere, in CCM, for 24 h. Then, CCM was replaced with other CCM with 1,000 μg/mL of particles with (MgPa-F) and without (MgPa) KF treatment and maintained in culture for 24 h.

Osteoblast and macrophages cell cultures were harvested by scraping to avoid the proteolysis of proteins by trypsin. Cell suspensions were lysed at 4°C by the addition of 1 × RIPA lysis buffer (Santa Cruz Biotechnology, Inc., Dallas TX, USA). After 1 h incubation at 4°C in the dark, samples were centrifuged at 5,000 g for 20 min at 4°C and the supernatants were recovered and stored at −20°C until use. Protein concentrations of the samples were determined using the DC protein assay kit from Bio-Rad. For each sample 50 μg of total proteins were analyzed in duplicate by 2D electrophoresis. The samples were processed and proteins were identified as described by Lozano et al. (2013).

Results

Turbulence by H_2 Bubbles and Corrosion Product Formation on the MgPa Surface

MgPa are corroded in the presence of a chloride-containing biological medium. The reported corrosion reaction steps include an increase in pH and formation of hydrogen bubbles (Mueller et al., 2009). The corrosion process was followed in real time by MM. The generation and detachment of bubbles (Fig. 1, circles) that induced displacement of the surrounding particles (arrows) could be followed by MM. Consequently, there was turbulence in the vicinity that probably affected the surrounding cells.

In the sequence of Supplementary Figure 1 it can be noticed that a gray layer (probably $Mg(OH)_2$, Mueller et al., 2009) progressively covered the MgPa.

Supplementary Figure 1

Supplementary Figure 1 can be found online. Please visit journals.cambridge.org/jid_MAM.

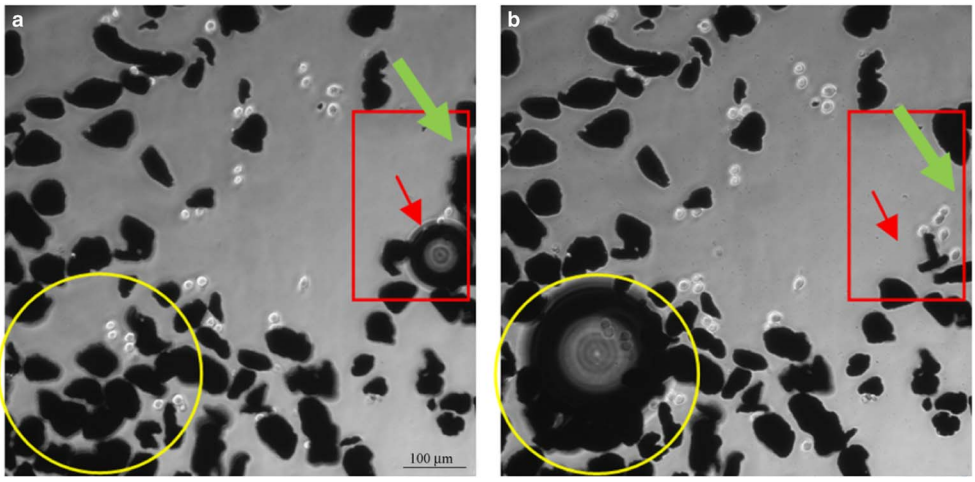

Figure 1. Time-lapse microphotographs showing the degradation process of MgPa (1,000 μg/mL) with bubble formation [see circles, bubble is absent in (**a**) and present in (**b**)] and detachment [see rectangles, bubble is present in (**a**) and absent in (**b**)] as well as displacement of some MgPa after bubble detachment (arrows).

Interaction of Macrophages with MgPa During the Corrosion Layer Formation

In the absence of MgPa particles, macrophages grow normally. An increase in cell number in the 24 h assay was detected, as observed in Supplementary Figure 2.

A different cellular behavior was noticed when MgPa were added to the cell culture (sequence of Fig. 2, supplementary information in Supplementary Fig. 3). Some macrophages closely interacted with the corrosion products, moved the position of the particles (cells contacted the particles and particles were slowly moved), and displayed cellular morphological changes. The initial condition is shown in Figure 2a. Bright cells and particles without corrosion products can be seen. In Figure 2b one of the cells on the right died and the division process can be observed in the other cell. In addition, bright corrosion products can be detected on the borders of some of the MgPa. In the same Figure two cells can be clearly distinguished on the right and four in the center due to the division process. These cells interact with the MgPa and with submicron particles of the surrounding area. In Figure 2c (left side) morphological changes and cell damage can be noticed after cell/MgPa contact. Subsequently, all the cells on the right died (Fig. 2d). When Figures 2a and 2d are compared it can be noticed that the position of some of MgPa changed after the interaction with cells (no bubble formation associated with movement of the MgPa was detected in this frame). Figure 2d shows cells that seem to be alive, but are smaller and more shadowy than those of the initial $t = 0$ time (Fig. 2a). Some cells that were not very close to the particles also died a few minutes after their duplication.

Supplementary Figures 2 and 3

Supplementary Figures 2 and 3 can be found online. Please visit journals.cambridge.org/jid_MAM.

Interaction of Macrophages with Submicron Particles

The interaction of macrophages with MgPa and MgPa-F was also observed in the assays. Successive stretching and retracting processes of pseudopodia to engulf submicron particles could be followed by the time-lapse sequence in both cases (Fig. 3).

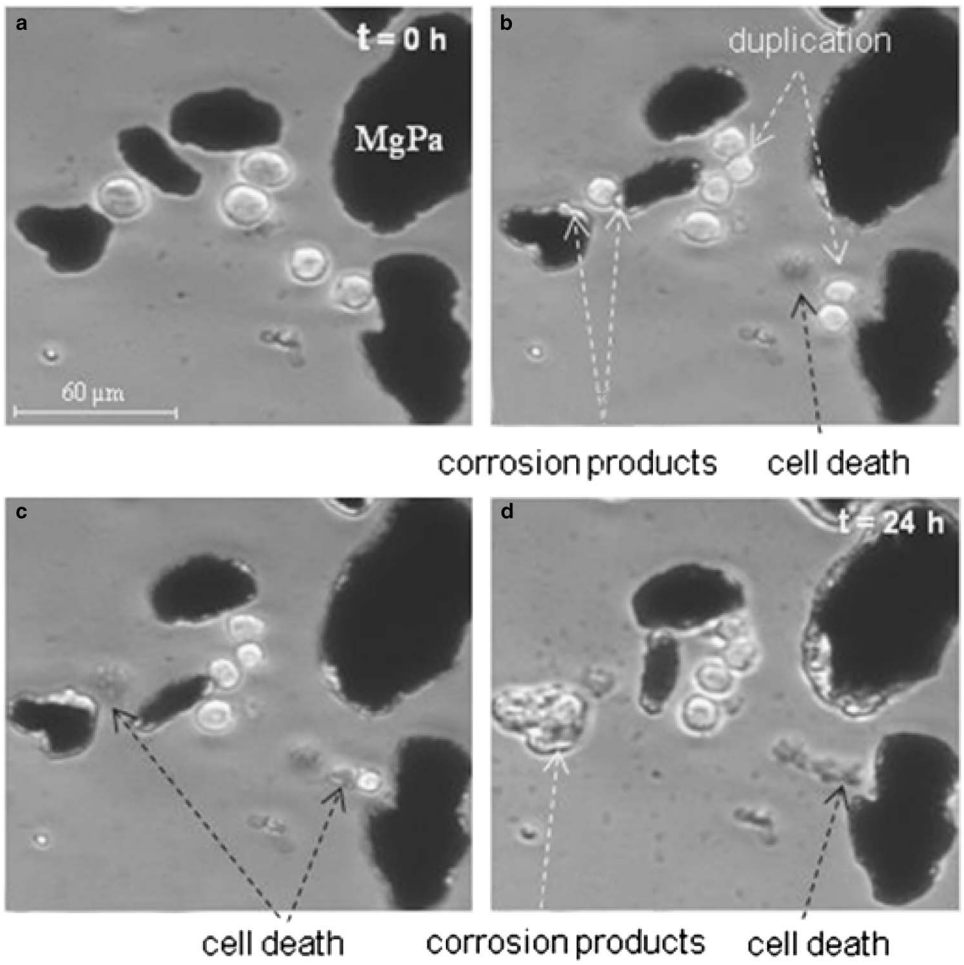

Figure 2. Time-lapse microphotographs of J774 macrophages in contact with 1,500 μg/mL MgPa during a 24 h assay: Interaction of macrophages with MgPa, duplication of cells, displacement of particles by the cells, formation of corrosion products on the surface, and cell death can be detected within the sequence (**a–d**) (see also Supplementary Fig. 3).

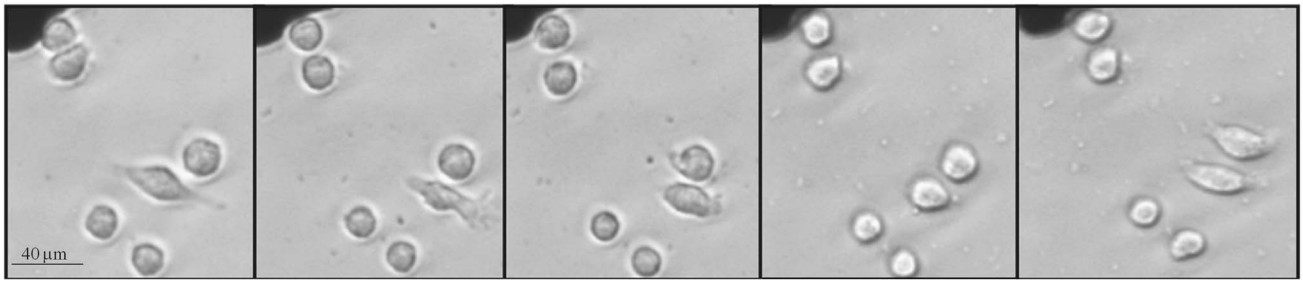

Figure 3. Time-lapse microphotographs showing the interaction of J774 macrophages with submicron MgPa during 1,500 μg/mL MgPa-F assay. The stretching and retracting of macrophage pseudopodia to engulf microparticles can be seen, the process is repeated over the exposure period.

Alterations of Cell Cycles and Viability of J774 and MC3T3-E1

To complement the microscopy observations, cell cycles of J774 and MC3T3-E1 cell lines were studied by FC and a qualitative comparison is reported here (Table 2). We wanted to know if different cell lines were similarly affected by the presence of the MgPa and MgPa-F. Our results show considerable differences for both cell line cycles when results with and without particles are compared. However, they are more meaningful in the case of macrophages. Thus, when MgPa were present, the $SubG_1$ phase increase (with respect to the control) was higher for J774 than for MC3T3-E1. Conversely, when MgPa were present, the S phase markedly decreased in J774, while for MC3T3-E1 it remained close to the control value.

Notable differences in cell cycle phases after exposure to MgPa-F were also observed. Comparing results with those obtained for MgPa and the respective control (Table 2) in the case of macrophages exposure to MgPa-F particles produced an important increase in the percentage of cells in SubG1 phase and a substantial decrease in S phase. No meaningful changes were observed in the case of osteoblasts.

Relative viability of both cell lines decreased in the presence of particles with macrophages being more sensitive than osteoblasts, showing the lowest viability value in the presence of MgPa-F. Consequently, the response of these two cell lines was different when they were exposed to the particles.

In agreement, analysis of the microphotographs obtained by MM in real time revealed a high decrease in the number of cells during exposure to MgPa or MgPa-F (Table 2, Figs. 2 and 4). Interestingly, it can be noticed that cells that were close to corroding particles (squares) were seriously damaged while those that were far from the corroding area were not significantly altered (circles in Figs. 4a and 4b). The slow movement of particles by the cells could also be observed (Fig. 4, rectangles recorded at the initial and final positions after several minutes of movement).

Alteration of the MC3T3-E1 Adhesion Process by MgPa: CIM

The adhesion process is frequently analyzed when the interaction of cells with biomaterials is studied (Zachman et al., 2013). During the harvesting step it was noticed that removal of M3C3T3-E1 cells using trypsin to obtain cell suspensions was more difficult in cells growing with MgPa. Under this condition these cells showed stronger resistance to removal than those without particles that could be detached easily. Consequently, these changes may suggest alterations in the adhesion process in the presence of MgPa.

CIM was used to make a qualitative investigation about the influence of the presence of MgPa on cell adhesion to the substrate. For this assay, osteoblasts (MC3T3-E1) were first incubated with the primary antibodies (anti-ICAM-1 and anti-vimentin) and subsequently with the fluorescent secondary antibodies.

Micrographs obtained in the absence (left) and in the presence (right) of 1,000 μg/mL MgPa are shown in Figure 5. The cells were incubated with the primary antibodies to the adhesion protein ICAM-1 and the intermediate filament protein vimentin and the specific immune interaction was

Table 2. Cellular Effects of MgPa and MgPa-F (1,000 μg/mL) in the Different Cell Cycle Phases by Flow Cytometry.

Cell Line	MgPa Surface	$SubG_1$ (%)	G_1 (%)	S (%)	G_2/M (%)	Relative Viability (%)
MC3T3-E1	—	3.5	76.6	13.9	6.0	100
MC3T3-E1	MgPa	4.4	72.6	13.2	9.8	78.5
MC3T3-E1	MgPa-F	4.2	75.2	12.2	8.4	65.7
J774	—	3.2	64.6	20.0	12.2	100
J774	MgPa	8.3	84.2	1.7	5.8	65.0
J774	MgPa-F	14.8	71.2	7.6	6.4	35.1

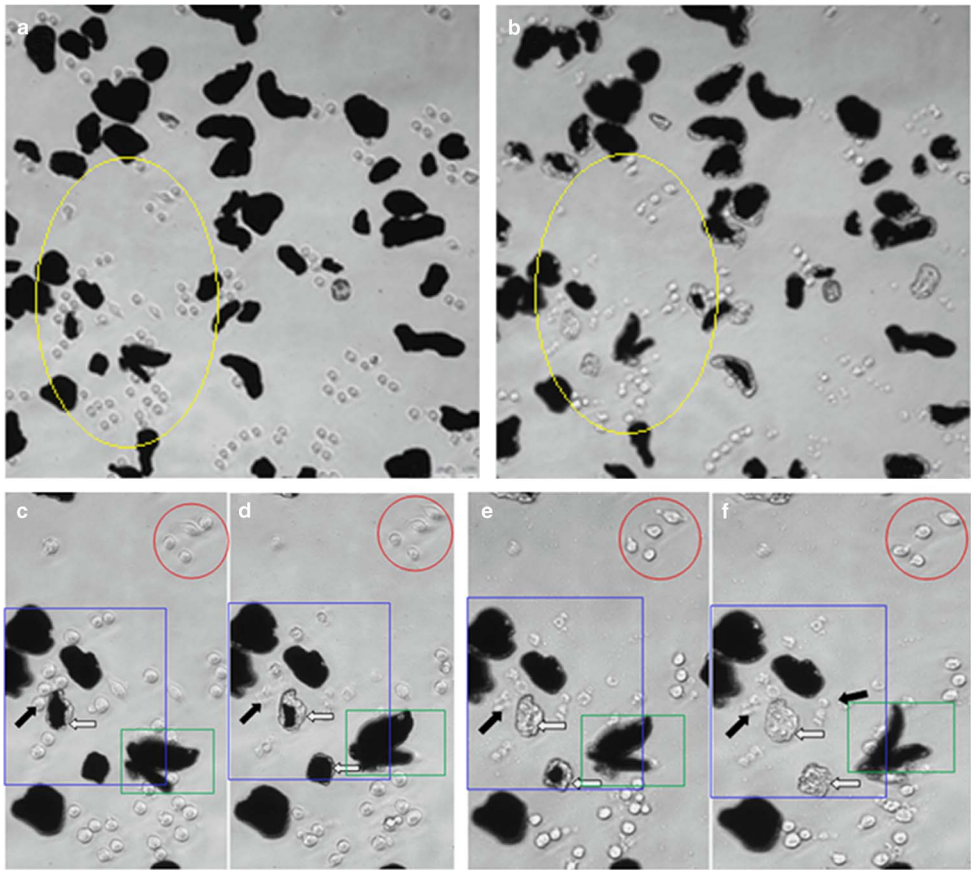

Figure 4. Time-lapse microphotographs of J774 (**a**) at the beginning (0 h) and (**b**) 24 h after the exposure to 1,000 μg/mL MgPa-F. Cell death can be detected in (**b**) (ellipses). Magnification (400×). **c-f:** Time-lapse microphotographs showing a detailed sequence for the region within the yellow ellipse. The gradual formation of corrosion products on MgPa-F surface (white arrows in the squares) and the cells progressively damaged in the surroundings (black arrows) can be noticed. Those cells that are far from the corroded particles are unaltered (circles) and interact with the submicron particles of the surrounding area. Macrophages are able to change the position of the particles (rectangles). Magnification (1,000×).

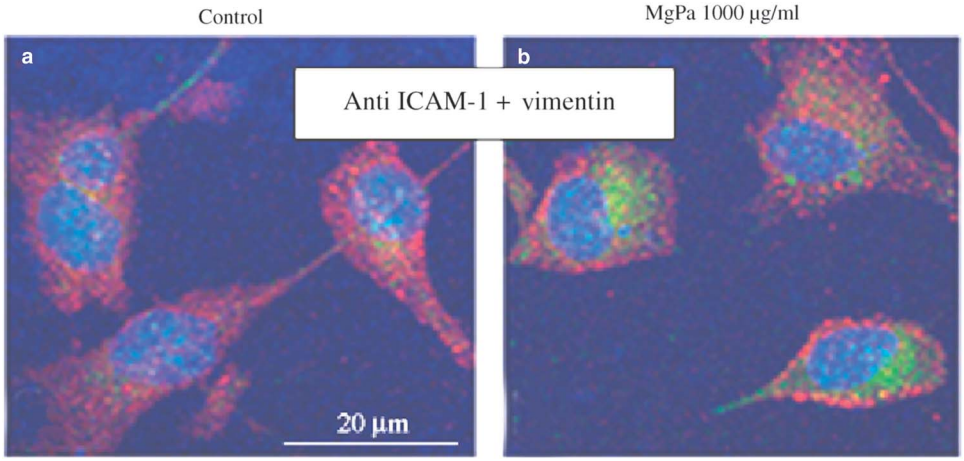

Figure 5. MC3T3-E1 immunofluorescence studies. Dual staining and detection by confocal microscopy of ICAM-1 (green) and vimentin (red) (**a**) MC3T3-E1 cultures in the absence of MgPa (control) and (**b**) MC3T3-E1 cultures in the presence of 1,000 μg/mL MgPa (see also Supplementary Fig. 5).

detected by the respective secondary antibodies (green for ICAM-1 and red for vimentin), as described above. The results obtained for dual detection of anti-ICAM-1 and anti-vimentin are shown in Figure 5 (see Supplementary Fig. 4 for individual detection of ICAM-1 and vimentin). It can be noticed that cells exposed to MgPa showed

differences in the expression of the ICAM-1 and vimentin proteins involved in the mechanism of cell adhesion. Particularly, the expression of ICAM-1 (green) when cells were in contact with MgPa was particularly increased with respect to the control without particles.

Supplementary Figure 4

Supplementary Figure 4 can be found online. Please visit journals.cambridge.org/jid_MAM.

Proteomic Analysis Profile Before and After Exposure to MgPa

Proteomic profile analysis of cells under study was used to investigate the effect of MgPa on protein expression (Vandekerckhove & Weber, 1978; Alcaide et al., 2012). The analysis of J774 macrophage lysates in the absence and presence of MgPa (1,000 μg/mL) showed several differences between identified proteins from their peptide fingerprinting. After the exposure to MgPa, results showed differences in the expression of cytoskeletal proteins such as tubulin, γ-actin, and elongation factor glyceraldehyde-3-phosphate dehydrogenase (G3PDH) (Supplementary Table 1). Exposure to MgPa produced a decreased in tubulin and heat shock protein (HSP90 and HSP8) expression. On the other hand, γ-actin expression together with G3PDH and actin regulatory protein (isoform 2), increased after exposure to MgPa. A shift in the acidic direction of the isoelectric point of γ-actin was also observed.

Proteomic profile analysis of MC3T3-E1 lysates also showed changes in cytoskeletal proteins. In the presence of MgPa the expression of tubulin and peptide elongation factor 1 α1 decreased, while expression of γ-actin increased with a shift in the acidic direction (Supplementary Table 1).

Supplementary Table 1

Supplementary Table 1 can be found online. Please visit journals.cambridge.org/jid_MAM.

Comparison of LDH and WST-1 Assays for J774 and MC3T3-E1 with MgPa and MgPa-F

Figure 6 shows a marked difference in the levels of LDH for J774 and MC3T3-E1 cell lines in response to MgPa presence (24 h exposure). A concentration-dependent impact with high deleterious effect for J774 in contact with MgPa for concentrations ≥1,000 μg/mL was found, while MC3T3-E1 cells were not significantly affected (Fig. 6a).

Alternatively, WST-1 assay showed concentration-dependent adverse effects for both J774 and MC3T3-E1 cell lines (Fig. 6b). A significant decrease in mitochondrial activity was found for concentrations ≥500 μg/mL that were more detrimental in J774 cells (≤25% for ≥1,500 μg/mL).

Damage to cell membranes was dependent on the concentration of particles when certain threshold values were exceeded, both, in the presence and absence of F-coating on the particles. Thus, in J774 cells after exposure to MgPa-F significant damage was found for concentrations ≥1,000 μg/mL that was less deleterious than for exposures to MgPa (Fig. 6a). MC3T3-E1 cells were affected at 2,000 μg/mL MgPa-F.

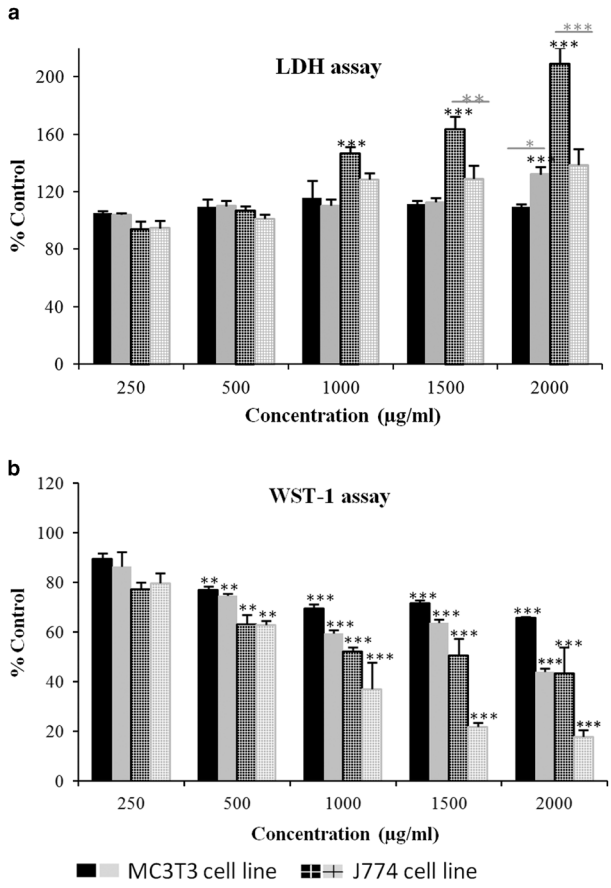

Figure 6. Effects after 24 h exposure to different concentrations of MgPa (black) and MgPa-F (gray) on plasma membrane integrity evaluated by lactase dehydrogenase (LDH) activity (**a**) and cell proliferation measured by mitochondrial respiratory activity, evaluated by WST-1 (**b**). Significant difference at $^{***}p < 0.001$ without particles vs with MgPa; $\underline{^{***}}\,p < 0.001$; $\underline{^{**}}\,p < 0.01$; $\underline{^{*}}\,p < 0.05$ MgPa vs MgPa-F.

WST-1 assay showed concentration-dependent adverse effects for both J774 and MC3T3-E1 (Fig. 6b). A more important decrease in mitochondrial activity was found for concentrations ≥1,000 μg/mL in case of J774 in contact with MgPa-F than after exposures to MgPa.

Discussion

Biocompatibility of Mg-based materials is frequently analyzed by employing extracts obtained from Mg degradation (Mao et al., 2013; Scheideler et al., 2013; Yang et al., 2013). However, this type of assay does not provide information about the interaction of cells with particles and corrosion products that are gradually formed *in situ*

(Di Virgilio et al., 2011; Grillo et al., 2011). Degradation of Mg and interaction with cells was previously analyzed *ex situ* (Zhang et al., 2009). Formation of $Mg(OH)_2$ and hydroxyapatite of Mg and Mg-based alloys was reported. In a previous work we have shown that MgPa degraded and affected the growth of osteoblastic cells in culture (Di Virgilio et al., 2011). To achieve a better understanding of the processes occurring at the particle/cell interface *in situ* a real time evaluation was made by MM to assess macrophage response after exposure to particles, allowing the simultaneous evaluation of corrosion processes in particles and the concomitant cellular response. These observations were complemented by other biological assays including CIM to test effects of the Mg particles on cells and the corrosion products derived from them.

The gradual corrosion of MgPa that were progressively covered by a gray layer that may be $Mg(OH)_2$ (Mueller et al., 2009) could be followed by MM. In addition, formation of hydrogen bubbles, derived from Mg degradation (Kirkland, 2012), that generated turbulence and moved the position of particles could also be detected. Marked differences between the J774 control cells and those exposed to MgPa were noticed. A decrease in the cell number and an important number of dead cells were observed when the particles were present. Several macrophages closely interacted with MgPa and MgPa-F displayed changes in size morphology and brightness. Interactions of cells with larger MgPa resulted in cell damage and eventually led to their death, particularly in areas where MgPa were corroding. Repeated stretching and retracting processes of pseudopodia to engulf submicron particles could also be followed by the time-lapse sequence of MM in both MgPa and MgPa-F. Cells do not seem to be affected after these processes. Meanwhile, cells of the control assay, without particles, divided and remained bright and alive during the whole observation time.

The results of cell cycle and viability tests during exposure to the particles were provided to complement MM information and to identify biological alterations. Important changes were observed after exposure to 1,000 μg/mL MgPa: macrophage viability decreased greatly, SubG1 increased, while the S phase decreased. As described previously (Luo et al., 2014) the SubG1 population is indicative of apoptotic cells. Exposure of macrophages to MgPa for 24 h induced an apoptotic response that finally led to cell death, probably due to changes induced by the corrosion process: pH increase, release of corrosion products, and bubble formation with concomitant turbulence.

Proteomic profile analysis revealed a significant change in the γ-actin expression pattern in the presence of MgPa in osteoblast and macrophage cell lysates. In both cell cultures, an increase in the expression of a form of this protein with a lower Ip was detected. γ-actin acidification has been related to alterations in the cell cytoskeleton as well as changes in cell morphology (Lozano et al., 2013). Actin is a monomeric subunit of cytoskeleton microfilaments, and its polymerization provides structural support and regulates contractility, cytokinesis, phagocytosis, adhesion, and cell morphology (Vandekerckhove & Weber, 1978). It's polymerization is dependent on the presence of Ca and Mg cations (Vandekerckhove & Weber, 1978; Bergeron et al., 2010). These proteins are also very important in the mobility of migratory cells, which modify the actin filaments forming lamellipodia with free extensions called filopodia. Lamellipodia are frequently developed by osteoblastic cells growing on rough surfaces (Sawase & Watanabe, 2015). Consequently, alterations in the adhesion process may be related to change in γ-actin expression by the presence of MgPa. These results were complemented by those obtained with CIM, whereby differences were visualized in the expression of proteins such as ICAM-1 and vimentin related to adhesion processes.

It is known that ICAM-1 is an intercellular adhesion protein, associated with the cytoskeleton, which is involved in intracellular signaling activation. Vimentin is a protein of the intermediate filaments that forms the cell cytoskeleton and contributes to support of cell membranes. Osteoblasts adhere to opposing cells through these particular adhesion molecules (vimentin and ICAM-1) on their surface and these adhesion molecules not only function as glue with opposing partners but transduce activation signals that facilitate the production of bone-resorbing cytokines (Tanaka et al., 1995). Thus, alterations in vimentin and ICAM-1 expression by the presence of MgPa detected by CIM are probably related to changes in the adhesion process. They may be promoted by Mg ions that possibly mediate the adhesion of cells to the substrate, probably by decreasing the negative charge of the surface, hence reducing the surface repulsive electrostatic forces (Takeichi & Okada, 1972; Kleine et al., 2003).

To test the influence of other ions on the biological response of cells, experiments with MgPa treated with KF were made. A weak protection of the F-containing layer was confirmed by MM. The corrosion process was noticed in several particles that were progressively covered by corrosion products, similarly to those observed in case of MgPa. In addition, higher reduction in the viability of cells than that observed in the control cells or in those cells exposed to MgPa was detected during cells/MgPa-F MM observations. This deleterious effect was followed by other techniques to complement MM information. Results showed changes in all phases of the cell cycle as well as in viability of macrophages after exposure to 1,000 μg/mL MgPa-F. Cell numbers in the SubG1 phase increased and the S phase and viability decreased. Accordingly, it was observed that cells that were close to MgPa-F were strongly affected and alterations frequently led to the reduction of cell number with respect to the control and to cell death. However, the effect of MgPa-F on macrophages was more significant than that on MC3T3-E1, since viability of J774 was lower and cell cycle was more affected. Variations were more important than those observed after exposure to MgPa without treatment and, consequently, F-dependent effects may be related to them.

In this sense, F-ions do not affect lysosomal activity when added up 1×10^{-3} M to the cell culture as KF

(Grillo et al., 2011). However, the present results seem to indicate that in the case of MgPa-F either F^- local concentration (close to the particles) may be high ($\geq 1 \times 10^{-3}$ M) at certain sites or the products of their interaction with Mg affect mitochondrial activity and, ultimately, cell proliferation. It is known that F^- may induce oxidative stress and damage at the DNA level (Zhang et al., 2008). Free radicals can enter the cell nucleus and cause changes in the DNA, such as chain breaks. Furthermore, F^- can form covalent bonds with mammalian DNA and cause damage at the cellular level (Guo et al., 2003; Gutowska et al., 2010). It has been reported that incubation of THP-1 macrophages in F^--containing solutions cause a decrease in ATP synthesized by the cells and an increase in the formation of reactive oxygen species. Besides, an increase in cell death after the increase in F^-concentration in the medium was noticed. It was suggested that F^- could destabilize normal functioning of the cell respiratory chain, which induce lipid peroxidation and apoptosis of cells (Hirano & Suzuki, 1996; Wang et al., 2004). In addition, cytotoxic effects of F^- in rat alveolar macrophages was also reported while Anuradha et al. (2000) argued that F^- causes the activation of kinases that induce apoptosis. Gong et al. (2014) studied the effect of F^- on the viability of MC3T3-E1 cells and reported that NaF reduced cell viability in a concentration-dependent manner and promotes apoptosis. They suggest that this is due to the direct action of F^- on the expression of the proteins of the bcl-2 family.

It is known that treatments with KF are weakly protective unlike other treatments with HF (Wolters et al., 2015). Pereda et al. (2011) reported that when KF treated MgPa are immersed in chloride-containing media, chloride ions induce the dissolution of the F-containing layer, and subsequently the F content of the layer decreases. Thus, the layer becomes more labile to corrosion attack, corrosion products are formed and fluoride-containing ions are released together with Mg ions. Thus, changes in the biological activity of cells after exposure to MgPa-F in relation to exposures to MgPa without treatment could be related to the release of F-containing degradation products.

Conclusions

To achieve a better understanding of the processes occurring at the biodegradable metallic debris/cell interface *in vivo*, MM evaluation of corrosion processes in Mg-based particles and alterations of the surrounding cells was made. Development of hydrogen bubbles with concurrent turbulence and formation of Mg-based corrosion products covering the particles were detected. These effects, probably together with pH changes and Mg and F^- ion release (MgPa-F), induced changes in the surrounding cells. MM evaluations made in real time, *in situ* provided important information about the biodegradation of biomaterials that could not be obtained using extracts. This MM analysis was complemented by other assays to test cell response.

The behavior of macrophages and osteoblasts were compared. Complementary measurements showed alterations in cell cycle, changes in proteomic profile in proteins implicated in adhesion processes, and in cell number and viability. These changes were sometimes more significant in MgPa-F covered by a poorly protective fluoride layer. This more deleterious effect was probably due to the F^- containing species released during the corrosion process. Interaction of macrophages with the particles was more deleterious than in case of osteoblasts. These results were in agreement with the MM information, demonstrating that this technique is a helpful tool for monitoring changes in biodegradable materials and the surrounding cells during the degradation process in real time and *in situ*, and to achieve a better simulation of the interaction of debris with cells *in vivo*.

Acknowledgments

R.M.L.P. and B.P.M. wish to thank Dr. Pedro Lastres and Amadeo Cazaña for technical assistance in flow cytometry assays and data analysis, and to Dr. Vivian de los Ríos and Dr. Francisco García-Tabares for technical assistance in 2D-electrophoresis assays and protein identification by MALDI Peptide Mass Fingerprinting and Database Searching. The authors also wish to thank María Teresa Seisdedos and Maria Gema Elvira for excellent technical assistance in multidimensional microscopy *in vivo* assays. Contract grant sponsor: Ministerio de Ciencia e Innovación; contract grant number: MAT2008-06719-C03-01-02. Contract grant sponsor: Ministerio de Economía y Competitividad from Spain; contract grant number: MAT2011-29152-C02-02. C.G. and M.F.L.M acknowledge the sponsorship of CONICET, UNLP (11/I163), and ANPCyT (PICT 2010-1779; PICT 2012-1795 and PPL 2011 0003).

References

Alcaide, M., Ramírez-Santillán, C., Feito, M.J., De La Concepción Matesanz, M., Ruiz-Hernández, E., Arcos, D., Vallet-Regí, M. & Portolés, M.T. (2012). In vitro evaluation of glass-glass ceramic thermoseed-induced hyperthermia on human osteosarcoma cell line. *J Biomed Mater Res A* **100A**(1), 64–71.

Anuradha, C.D., Kanno, S. & Hirano, S. (2000). Fluoride induces apoptosis by caspase-3 activation in human leukemia HL-60 cells. *Arch Toxicol* **74**(4–5), 226–230.

Badar, M., Lünsdorf, H., Evertz, F., Rahim, M.I., Glasmacher, B., Hauser, H. & Mueller, P.P. (2013). The formation of an organic coat and the release of corrosion microparticles from metallic magnesium implants. *Acta Biomater* **9**(7), 7580–7589.

Baradez, M.-O. & Marshall, D. (2011). The use of multidimensional image-based analysis to accurately monitor cell growth in 3D bioreactor culture. *PLoS One* **6**(10), e26104.

Bergeron, S.E., Zhu, M., Thiem, S.M., Friderici, K.H. & Rubenstein, P.A. (2010). Ion-dependent polymerization differences between mammalian β- and γ-nonmuscle actin isoforms. *J Biol Chem* **285**(21), 16087–16095.

Bondarenko, A., Hewicker-Trautwein, M., Erdmann, N., Angrisani, N., Reifenrath, J. & Meyer-Lindenberg, A. (2011). Comparison of morphological changes in efferent lymph nodes after implantation of resorbable and non-resorbable implants in rabbits. *Biomed Eng* **10**, 32.

Bondarenko, A., Hewicker-Trautwein, M., Erdmann, N., Angrisani, N., Reifenrath, J., & Meyer-Lindenberg, A. (2011). Comparison of morphological changes in efferent lymph nodes after implantation of resorbable and non-resorbable implants in rabbits. *BioMedical Engineering OnLine* 10, 32. http://doi.org/10.1186/1475-925X-10-32

Caicedo, M.S., Desai, R., McAllister, K., Reddy, A., Jacobs, J.J. & Hallab, N.J. (2009). Soluble and particulate Co-Cr-Mo alloy implant metals activate the inflammasome danger signaling pathway in human macrophages: A novel mechanism for implant debris reactivity. *J Orthop Res* **27**(7), 847–854.

Collins, T.J. (2007). ImageJ for microscopy. *BioTechniques* **43** (Suppl 1), 25–30.

Davis, R.G., Goodman, S.B., Smith, R.L., Lerman, J.A. & Williams Iii, R.J. (1993). The effects of bone cement powder on human adherent monocytes/macrophages in vitro. *J Biomed Mater Res* **27**(8), 1039–1046.

Di Virgilio, A.L., Reigosa, M. & De Mele, M.F.L. (2011). Biocompatibility of magnesium particles evaluated by in vitro cytotoxicity and genotoxicity assays. *J Biomed Mater Res B Appl Biomater* **99B**(1), 111–119.

Doyle, A., Griffiths, J.B. & Newell, D.G. (1995). *Testing for Microbial Contamination*. West Sussex, England: John Wiley & Sons Ltd.

Dumbleton, J.H. (1981). *Tribology of Natural and Artificial Joints*. Amsterdam, The Netherlands: Elsevier Science Publishing Co.

Freeman, M.A.R., Bradley, G.W. & Revell, P.A. (1982). Observations upon the interface between bone and polymethylmethacrylate cement. *J Bone Joint Surg B* **64**(4), 489–493.

Gelb, H., Schumacher, H.R., Cuckler, J. & Baker, D.G. (1994). In vivo inflammatory response to polymethylmethacrylate particulate debris: Effect of size, morphology, and surface area. *J Orthop Res* **12**(1), 83–92.

Glant, T.T. & Jacobs, J.J. (1994). Response of three murine macrophage populations to particulate debris: Bone resorption in organ cultures. *J Orthop Res* **12**(5), 720–731.

Goldring, S.R., Clark, C.R. & Wright, T.M. (1993). The problem in total joint arthroplasty: Aseptic loosening. *J Bone Joint Surg A* **75**(6), 799–801.

Gong, X., Fan, Y., Zhang, Y., Luo, C., Duan, X., Yang, L. & Pan, J. (2014). Inserted rest period resensitizes MC3T3-E1 cells to fluid shear stress in a time-dependent manner via F-actin-regulated mechanosensitive channel(s). *Biosci Biotechnol Biochem* **78**(4), 565–573.

Goodman, S.B., Knoblich, G., O'Connor, M., Song, Y., Huie, P. & Sibley, R. (1996). Heterogeneity in cellular and cytokine profiles from multiple samples of tissue surrounding revised hip prostheses. *J Biomed Mater Res* **31**(3), 421–428.

Grillo, C.A., Alvarez, F. & de Mele, M.A. (2011). Biological effects of magnesium particles degradation on UMR-106 cell line: Influence of fluoride treatments. *Colloids Surf B Biointerfaces* **88**(1), 471–476.

Gu, X.N., Xie, X.H., Li, N., Zheng, Y.F. & Qin, L. (2012). In vitro and in vivo studies on a Mg-Sr binary alloy system developed as a new kind of biodegradable metal. *Acta Biomater* **8**(6), 2360–2374.

Guo, X.Y., Sun, G.F. & Sun, Y.C. (2003). Oxidative stress from fluoride-induced hepatotoxicity in rats. *Fluoride* **36**(1), 25–29.

Gutowska, I., Baranowska-Bosiacka, I., Baśkiewicz, M., Milo, B., Siennicka, A., Marchlewicz, M., Wiszniewska, B., Machaliński, B. & Stachowska, E. (2010). Fluoride as a pro-inflammatory factor and inhibitor of ATP bioavailability in differentiated human THP1 monocytic cells. *Toxicol Lett* **196**(2), 74–79.

Harris, W.H., Schiller, A.L., Scholler, J.M., Freiberg, R.A. & Scott, R. (1976). Extensive localized bone resorption in the femur following total hip replacement. *J Bone Joint Surg A* **58**(5), 612–618.

Hart, A.J., Quinn, P.D., Sampson, B., Sandison, A., Atkinson, K.D., Skinner, J.A., Powell, J.J. & Mosselmans, J.F.W. (2010). The chemical form of metallic debris in tissues surrounding metal-on-metal hips with unexplained failure. *Acta Biomater* **6**(11), 4439–4446.

Held, M., Schmitz, M.H.A., Fischer, B., Walter, T., Neumann, B., Olma, M.H., Peter, M., Ellenberg, J. & Gerlich, D.W. (2010). CellCognition: Time-resolved phenotype annotation in high-throughput live cell imaging. *Nat Met* **7**(9), 747–754.

Hirano, S. & Suzuki, K.T. (1996). Exposure, metabolism, and toxicity of rare earths and related compounds. *Environ Health Perspect* **104**(Suppl 1), 85–95.

Horowitz, S.M., Frondoza, C.G. & Lennox, D.W. (1988). Effects of polymethylmethacrylate exposure upon macrophages. *J Orthop Res* **6**(6), 827–832.

Horowitz, S.M. & Gonzales, J.B. (1996). Inflammatory response to implant particulates in a macrophage/osteoblast coculture model. *Calcif Tissue Int* **59**(5), 392–396.

Horowitz, S.M. & Purdon, M.A. (1995). Mechanisms of cellular recruitment in aseptic loosening of prosthetic joint implants. *Calcif Tissue Int* **57**(4), 301–305.

Huth, J., Buchholz, M., Kraus, J.M., Mølhave, K., Gradinaru, C., Wichert, G.V., Gress, T.M., Neumann, H. & Kestler, H.A. (2011). TimeLapseAnalyzer: Multi-target analysis for live-cell imaging and time-lapse microscopy. *Comp Met Prog Biomed* **104**(2), 227–234.

Jasty, M.J., Floyd Iii, W.E., Schiller, A.L., Goldring, S.R. & Harris, W.H. (1986). Localized osteolysis in stable, non-septic total hip replacement. *J Bone Joint Surg A* **68**(6), 912–919.

Johanson, N.A., Bullough, P.G., Wilson, P.D. Jr, Salvati, E.A. & Ranawat, C.S. (1987). The microscopic anatomy of the bone-cement interface in failed total hip arthroplasties. *Clin Orthop Relat Res* **218**, 123–135.

Kang Jung, K., Chiba, J. & Rubash, H.E. (1994). In vivo and in vitro analysis of membranes from hip prostheses inserted without cement. *J Bone Joint Surg A* **76**(2), 172–180.

Kirkland, N.T. (2012). Magnesium biomaterials: Past, present and future. *Corrosion Eng Sci Technol* **47**(5), 322–328.

Kleine, Z., Fairchild, A., Shi, B., Kuhn, T.B. & Liang, H. (2003). Cell adhesion in biomaterials—An introduction. *58th STLE Annual Meeting*, New York, April 28–May 1.

Lind, M., Trindade, M.C.D., Yaszay, B., Goodman, S.B. & Smith, R.L. (1998). Effects of particulate debris on macrophage-dependent fibroblast stimulation in coculture. *J Bone Joint Surg B* **80**(5), 924–930.

Lozano, R.M., Pérez-Maceda, B.T., Carboneras, M., Onofre-Bustamante, E., García-Alonso, M.C. & Escudero, M.L. (2013). Response of MC3T3-E1 osteoblasts, L929 fibroblasts, and J774 macrophages to fluoride surface-modified AZ31 magnesium alloy. *J Biomed Mater Res A* **101**(10), 2753–2762.

Luo, X.J., Qin, Q.P., Li, Y.L., Liu, Y.C., Chen, Z.F. & Liang, H. (2014). Three platinum(II) complexes of 2-(methoxy-phenyl)-imidazo-[4,5-f]-[1,10] phenanthroline: Cell apoptosis induction by sub-G1 phase cell cycle arrest and G-quadruplex binding properties. *Inorg Chem Commun* **46**, 176–179.

Maloney, W.J. & Smith, R.L. (1995). Periprosthetic osteolysis in total hip arthroplasty: The role of particulate wear debris. *J Bone Joint Surg Ser A* **77**(9), 1448–1461.

Mao, L., Yuan, G., Niu, J., Zong, Y. & Ding, W. (2013). In vitro degradation behavior and biocompatibility of Mg-Nd-Zn-Zr alloy by hydrofluoric acid treatment. *Mater Sci Eng C* **33**(1), 242–250.

Mirra, J.M., Amstutz, H.C., Matos, M. & Gold, R. (1976). The pathology of the joint tissues and its clinical relevance in prosthesis failure. *Clin Orthop* **117**, 221–240.

Mueller, W.D., Lorenzo De Mele, M.F., Nascimento, M.L. & Zeddies, M. (2009). Degradation of magnesium and its alloys: Dependence on the composition of the synthetic biological media. *J Biomed Mater Res A* **90**(2), 487–495.

Nakashima, Y., Sun, D.H., Trindade, M.C.D., Maloney, W.J., Goodman, S.B., Schurman, D.J. & Smith, R.L. (1999). Signaling pathways for tumor necrosis factor-α and interleukin-6 expression in human macrophages exposed to titanium-alloy particulate debris in vitro. *J Bone Joint Surg A* **81**(5), 603–615.

Ogunbileje, J.O., Nawgiri, R.S., Anetor, J.I., Akinosun, O.M., Farombi, E.O. & Okorodudu, A.O. (2014). Particles internalization, oxidative stress, apoptosis and pro-inflammatory cytokines in alveolar macrophages exposed to cement dust. *Environ Toxicol Pharmacol* **37**(3), 1060–1070.

Pereda, M.D., Alonso, C., Gamero, M., Del Valle, J.A. & Fernández Lorenzo De Mele, M. (2011). Comparative study of fluoride conversion coatings formed on biodegradable powder metallurgy Mg: The effect of chlorides at physiological level. *Mater Sci Eng C* **31**(5), 858–865.

Posada, O.M., Tate, R.J. & Grant, M.H. (2015). Effects of CoCr metal wear debris generated from metal-on-metal hip implants and Co ions on human monocyte-like U937 cells. *Toxicol Vitro* **29**(2), 271–280.

Reddy, J.M., Latha, P., Gowda, B., Manvikar, V., Vijayalaxmi, D.B. & Ponangi, K.C. (2014). Smear layer and debris removal using manual Ni-Ti files compared with rotary Protaper Ni- Ti files—An in-vitro SEM study. *J Int Oral Health* **6**(1), 89–94.

Roth, I., Schumacher, S., Basler, T., Baumert, K., Seitz, J.-M., Evertz, F., Müller, P.P., Baümer, W. & Kietzmann, M. (2014). Magnesium corrosion particles do not interfere with the immune function of primary human and murine macrophages. *Prog Biomater* **4**(1), 21–30.

Santavirta, S., Konttinen, Y.T., Hoikka, V. & Eskola, A. (1991). Immunopathological response to loose cementless acetabular components. *J Bone Joint Surg B* **73**(1), 38–42.

Sawase, T. & Watanabe, I. (2015). Surface modification of titanium and its alloy by anodic oxidation for dental implant. In *Implant Surfaces and their Biological and Clinical Impact*, Wennerberg, A., Albrektsson, T., Jimbo, R. (Eds.), pp. 65–76. Berlin, Heidelberg: Springer.

Scheideler, L., Füger, C., Schille, C., Rupp, F., Wendel, H.P., Hort, N., Reichel, H.P. & Geis-Gerstorfer, J. (2013). Comparison of different in vitro tests for biocompatibility screening of Mg alloys. *Acta Biomater* **9**(10), 8740–8745.

Schmalzried, T.P., Maloney, W.J., Jasty, M., Kwong, L.M. & Harris, W.H. (1993). Autopsy studies of the bone-cement interface in well-fixed cemented total hip arthroplasties. *J Arthroplasty* **8**(2), 179–188.

Takeichi, M. & Okada, T.S. (1972). Roles of magnesium and calcium ions in cell-to-substrate adhesion. *Exp Cell Res* **74**(1), 51–60.

Tanaka, Y., Morimoto, I., Nakano, Y., Okada, Y., Hirota, S., Nomura, S., Nakamura, T. & Eto, S. (1995). Osteoblasts are regulated by the cellular adhesion through ICAM-1 and VCAM-1. *J Bone Miner Res* **10**(10), 1462–1469.

Trindade, M.C.D., Nakashima, Y., Lind, M., Sun, D.H., Goodman, S. B., Maloney, W.J., Schurman, D.J. & Smith, R.L. (1999). Interleukin-4 inhibits granulocyte-macrophage colony-stimulating factor, interleukin-6, and tumor necrosis factor-alpha expression by human monocytes in response to polymethylmethacrylate particle challenge in vitro. *J Orthop Res* **17**(6), 797–802.

Vandekerckhove, J. & Weber, K. (1978). At least six different actins are expressed in a higher mammal: An analysis based on the amino acid sequence of the amino-terminal tryptic peptide. *J Mol Biol* **126**(4), 783–802.

Wang, A.G., Xia, T., Chu, Q.L., Zhang, M., Liu, F., Chen, X.M. & Yang, K.D. (2004). Effects of fluoride on lipid peroxidation, DNA damage and apoptosis in human embryo hepatocytes. *Biomed Environ Sci* **17**(2), 217–222.

Wolters, L., Besdo, S., Angrisani, N., Wriggers, P., Hering, B., Seitz, J.M. & Reifenrath, J. (2015). Degradation behaviour of LAE442-based plate-screw-systems in an in vitro bone model. *Mater Sci Eng C* **49**, 305–315.

Yang, X., Li, M., Lin, X., Tan, L., Lan, G., Li, L., Yin, Q., Xia, H., Zhang, Y. & Yang, K. (2013). Enhanced in vitro biocompatibility/bioactivity of biodegradable Mg–Zn–Zr alloy by micro-arc oxidation coating contained Mg_2SiO_4. *Surf Coat Technol* **233**, 65–73.

Zachman, A.L., Page, J.M., Prabhakar, G., Guelcher, S.A. & Sung, H.J. (2013). Elucidation of adhesion-dependent spontaneous apoptosis in macrophages using phase separated PEG/polyurethane films. *Acta Biomater* **9**(2), 4964–4975.

Zhai, Z., Qu, X., Li, H., Yang, K., Wan, P., Tan, L., Ouyang, Z., Liu, X., Tian, B., Xiao, F., Wang, W., Jiang, C., Tang, T., Fan, Q., Qin, A. & Dai, K. (2014). The effect of metallic magnesium degradation products on osteoclast-induced osteolysis and attenuation of NF-κB and NFATc1 signaling. *Biomaterials* **35**(24), 6299–6310.

Zhang, M., Wang, A., Xia, T. & He, P. (2008). Effects of fluoride on DNA damage, S-phase cell-cycle arrest and the expression of NF-κB in primary cultured rat hippocampal neurons. *Toxicol Lett* **179**(1), 1–5.

Zhang, S., Li, J., Song, Y., Zhao, C., Zhang, X., Xie, C., Zhang, Y., Tao, H., He, Y., Jiang, Y. & Bian, Y. (2009). In vitro degradation, hemolysis and MC3T3-E1 cell adhesion of biodegradable Mg–Zn alloy. *Mater Sci Eng C* **29**(6), 1907–1912.